Citation for published version:
Rzhevskiy, AS, Guy, RH & Anissimov, YG 2016, 'Modelling drug flux through microporated skin', *Journal of Controlled Release*, vol. 241, pp. 194-199. https://doi.org/10.1016/j.jconrel.2016.09.029

DOI:
10.1016/j.jconrel.2016.09.029

Publication date:
2016

Document Version
Peer reviewed version

Link to publication

Publisher Rights
CC BY

University of Bath

Alternative formats
If you require this document in an alternative format, please contact:
openaccess@bath.ac.uk

General rights
Copyright and moral rights for the publications made accessible in the public portal are retained by the authors and/or other copyright owners and it is a condition of accessing publications that users recognise and abide by the legal requirements associated with these rights.

Take down policy
If you believe that this document breaches copyright please contact us providing details, and we will remove access to the work immediately and investigate your claim.

Download date: 05. May. 2023

Modelling drug flux through microporated skin

Alexey S. Rzhevskiy[1], Richard H. Guy[2] and Yuri G. Anissimov[3,*]

[1] School of Pharmacy, Griffith University, Gold Coast, Queensland, 4222, Australia.

[2] Department of Pharmacy & Pharmacology, University of Bath, Claverton Down, Bath, BA2 7AY, U.K.

[3] School of Natural Sciences, Griffith University, Gold Coast, Queensland, 4222, Australia.

[*] Correspondence: email: y.anissimov@griffith.edu.au, phone: +617 55528496

Running Head: Drug flux through porated skin

Abstract

A simple mathematical equation has been developed to predict drug flux through microporated skin. The theoretical model is based on an approach applied previously to water evaporation through leaf stomata. Pore density, pore radius and drug molecular weight are key model parameters. The predictions of the model were compared with results derived from a simple, intuitive method using porated area alone to estimate the flux enhancement. It is shown that the new approach predicts significantly higher fluxes than the intuitive analysis, with transport being proportional to the total pore perimeter rather than area as intuitively anticipated. Predicted fluxes were in good general agreement with experimental data on drug delivery from the literature, and were quantitatively closer to the measured values than those derived from the intuitive, area-based approach.

Keywords: percutaneous penetration, microporation, skin flux enhancement, mathematical modelling, transdermal drug delivery

Graphical Abstract

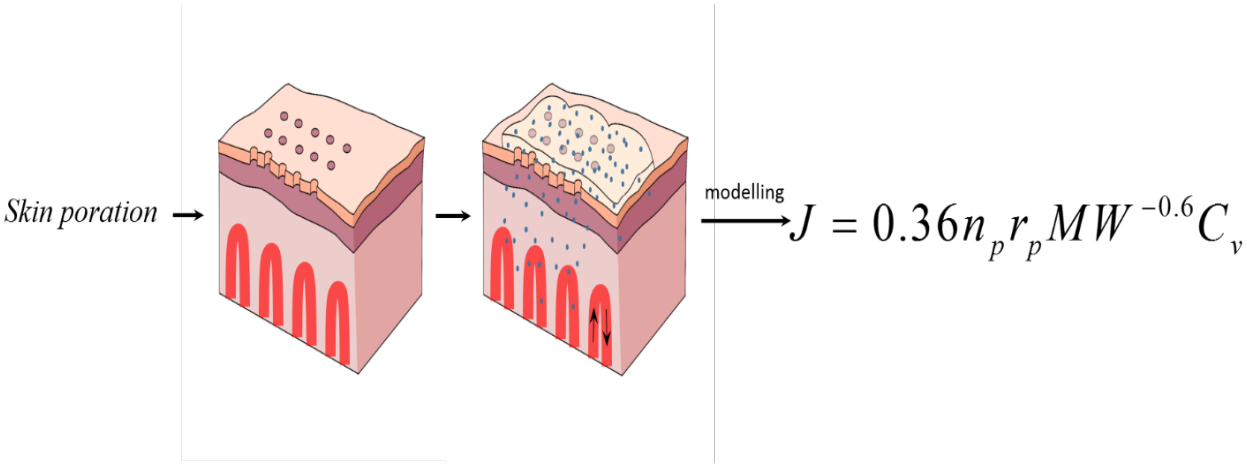

Introduction

The skin and its outer layer, the stratum corneum (SC), in particular, is a formidable barrier to the passive delivery of topical and transdermal drugs. The ideal physicochemical characteristics for 'good' skin penetrants are well-known: small molecular weight (MW), reasonable, but not excessive lipophilicity (log P = 2-3), adequate solubility in both oil and water, low melting point[1]. However, these criteria are seldom satisfied and, in essence, this has meant that the most successful drugs that are delivered into or through the skin for therapeutic effect are those with high pharmacological potency [2, 3].

The aim to deliver drugs requiring higher doses, or those with MW > 500 (e.g., peptides and small proteins), has led to a substantial effort to enhance percutaneous absorption, and to reversibly undermine skin barrier function, using a variety of different approaches [4]. Most recently, attention has focused on several so-called microporation techniques, based on the use of microneedles, laser poration and heat ablation to create entirely new pathways across the SC and circumvent thereby the major resistance to passive diffusion into the viable skin tissue [5, 6].

The underlying principle here is that (for example) large molecules will never transport through intact skin at a rate necessary to be useful therapeutically and it is therefore necessary to by-pass the SC. The microporation approaches do so by creating pores of 20-200 μm in diameter and of a depth that they are minimally invasive (i.e., as sensation-free as possible) [7, 8]. The strategy is reversible as the skin very effectively 'seals' itself quite quickly following such a disruption [9].

A key question when contemplating the application of a microporation technique to enhance topical/transdermal drug delivery is "how many pores, and of what dimension, are required to achieve the desired flux"? The simple, intuitive approach to make such a prediction is to assume

that the flux achieved will equal that through an aqueous domain, the surface area of which equals that of the total pore area created (and to assume that any contribution via intact SC is negligible). However, this logical assumption has not undergone rigorous testing and the possibility that the enhancement required may be achievable with fewer pores than intuitively expected (and hence rendering the approach even less invasive to the patient) has not been explored. In this paper, therefore, a model, based on water evaporation via leaf stomata [10, 11], for drug flux across the skin via micropores is developed and is compared both to the predictions from an intuitive, area-based model and to experimental measurements in the literature.

Model development

Following a poration event, it is assumed that round pores (of radius r_p), which completely penetrate the SC, are formed. It is further assumed that these pores are spaced at regular intervals as shown in Fig 1A, so that the pore density n_p (dimension: 1/cm^2 or pore number per cm^2) results in the spacing between the neighbouring pores of $l_p = 1/\sqrt{n_p}$. The applied drug concentration in the vehicle is maintained constant (C_v) over a distance h_v above the SC, while that at a depth h_s below the SC is assumed to be zero (i.e., sink conditions) as a result, for example, of clearance by the dermal microcirculation (see Fig 1B).

The steady state flux in the case that *all* of the SC barrier is removed may be expressed as:

$$J_{no\,SC} = C_v \left(\frac{h_v}{D_v} + \frac{h_s}{K_s D_s} \right)^{-1} \qquad \text{Eq 1}$$

where D_v and D_s are the drug's diffusivities in the vehicle and viable skin, respectively, and K_s is the partition coefficient of the drug between the viable skin and the vehicle. In the absence of SC, therefore, the diffusional resistance ($R_{no\,SC}$) to drug absorption is given by:

$$R_{no\,SC} = \frac{h_v}{D_v} + \frac{h_s}{K_s D_s} \qquad \text{Eq 2}$$

When the SC is only partially removed, an analytical solution to the diffusion equation cannot be obtained even for the steady state and an approach similar to that developed by Patlak [11] is therefore used to approximate the resistance in Eq. 1 by the integral:

$$R = \int_{-h_v}^{h_{sc}+h_s} \frac{dx}{K(x)D(x)a(x)} \qquad \text{Eq 3}$$

Here $K(x)$ and $D(x)$ are step functions describing drug partitioning and diffusion in the vehicle ($K(x)=1, D(x)=D_v$) and skin ($K(x)=K_s, D(x)=D_s$). Assuming that the SC pores are filled with the vehicle, then the partition and diffusion coefficients therein are the same as those in the vehicle ($K(x)=1, D(x)=D_v$). Further, in Eq 3, $a(x)$ is the fraction of the total area available for diffusion in the direction x; $a(x)$ is estimated by assuming that diffusion in the layers adjacent to the pores is limited to the region formed by the shaded "funnels" (see Fig 1B).

In terms of the geometry of these funnels, Patlak [11] has shown that $\tan\alpha \approx 4/\pi$. When the edges of neighbouring funnels intercept, as determined by the coordinates $x = h_{sc} + h_f$ and $x = -h_f$ on the skin and vehicle sides of the pore, respectively, and

$$h_f = \left(\tfrac{1}{2}l_p - r_p\right)/\tan\alpha = \pi\left(l_p - 2r_p\right)/8 \quad \text{for } x \geq h_{sc} + h_f \text{ or } x \leq -h_f ,$$

the available area of diffusion approximately equals the total area, and therefore $a(x)$ = 1.

Inside the pores ($0 \leq x \leq h_{sc}$) the fractional area available for diffusion is $a(x) = n_p \pi r_p^2$ while,

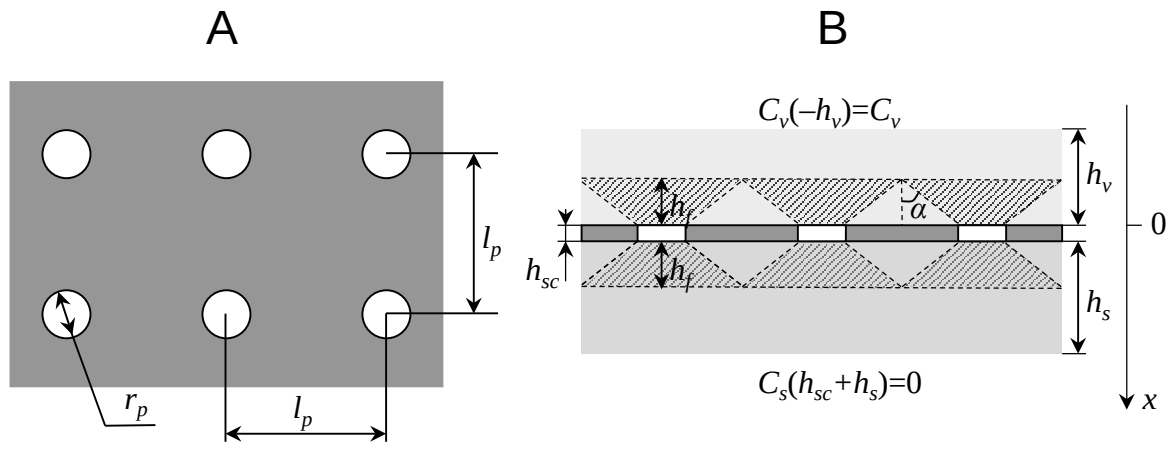

Fig 1. Schematic representation of pores in SC plane (A) and side view (B) with relevant dimensions defined in the text.

inside the funnels, $a(x) = n_p \pi r_f^2(x)$, where $r_f(x) = r_p + 4(x - h_{sc})/\pi$ for the skin side and $r_f(x) = r_p - 4x/\pi$ for the vehicle side. Thus, in summary, the functions $K(x), D(x)$ and $a(x)$ are given by:

$$K(x) = \begin{cases} 1, & \text{for } -h_v \le x \le h_{sc} \\ K_s, & \text{for } x > h_{sc} \end{cases} \quad ; \quad D(x) = \begin{cases} D_v, & \text{for } -h_v \le x \le h_{sc} \\ D_s, & \text{for } x > h_{sc} \end{cases}$$

$$a(x) = \begin{cases} 1, & \text{for } -h_v \le x \le -h_f \\ n_p \pi \left(r_p - 4x/\pi\right)^2, & \text{for } -h_f < x \le 0 \\ n_p \pi r_p^2, & \text{for } 0 < x \le h_{sc} \\ n_p \pi \left(r_p + 4(x - h_{sc})/\pi\right)^2, & \text{for } h_{sc} < x \le h_f + h_{sc} \\ 1, & \text{for } x > h_f + h_{sc} \end{cases} \qquad \text{Eq 4}$$

Substituting Eq 4 for $K(x), D(x)$ and $a(x)$ into the integral Eq 3 yields:

$$R = \int_{-h_v}^{-h_f} \frac{dx}{D_v} + \int_{-h_f}^{0} \frac{dx}{D_v n_p \pi \left(r_p - 4x/\pi\right)^2} + \int_{0}^{h_{sc}} \frac{dx}{D_v n_p \pi r_p^2} + \int_{h_{sc}}^{h_{sc}+h_f} \frac{dx}{K_s D_s n_p \pi \left(r_p + 4(x - h_{sc})/\pi\right)^2} + \int_{h_{sc}+h_f}^{h_{sc}+h_s} \frac{dx}{K_s D_s} \qquad \text{Eq 5}$$

With the assumption that both h_v and h_s are greater than or equal to h_f, integration of Eq 5 produces:

$$R = u(h_v - h_f)\frac{h_v - h_f}{D_v} + u(h_s - h_f)\frac{h_s - h_f}{K_s D_s} + \frac{h_{sc}}{D_v n_p \pi r_p^2} + \left(\frac{1}{D_v} + \frac{1}{K_s D_s}\right)\frac{l_p - 2r_p}{4 n_p l_p r_p} \qquad \text{Eq 6}$$

where $u(x)$ is the unit step function ($u(x) = 1$ if $x \ge 0$, and $u(x) = 0$ if $x < 0$). Given that $l_p = 1/\sqrt{n_p}$ and $h_f = \pi\left(l_p - 2r_p\right)/8$, the transport resistance R depends on parameters related to the drug, its vehicle and the skin (D_v, D_s and K_s), the pore density and radius (n_p and r_p), and the different layer thicknesses (h_v, h_s and h_{sc}).

While Eq 6 can be directly used to predict flux, for many practical cases of SC poration, further simplification is possible. First, it is reasonable to expect that the pore radius is much less than the distance between the pores ($2r_p \ll l_p$). Second, if the pore density is not large, such that $1/\left(4 n_p r_p\right) \gg h_s + h_v$, it follows that:

$$n_p \ll \frac{1}{4 r_p \left(h_s + h_v\right)} \qquad \text{Eq 7}$$

Hence, if the pore radius is comparable to the distance between the pores ($r_p \sim l_p$), or the pore density is equal to or greater than the right-hand side of Eq 7, then the first two terms in Eq 6 dominate the resistance which then approaches that in Eq 2, i.e., R_{noSC}. If, however, $2r_p \ll l_p$ and Eq 7 is satisfied, then the first two terms in Eq 6 can be neglected and:

$$R = \left[\frac{1}{D_v}\left(1+\frac{4h_{sc}}{\pi r_p}\right)+\frac{1}{K_s D_s}\right]\frac{1}{4n_p r_p} \qquad \text{Eq 8}$$

Eq 8 is a valid approximation as long as R is significantly greater than R_{noSC} (defined in Eq 2). The reciprocal of the resistance in Eq 8 is, of course, the drug's permeability coefficient across the porated skin:

$$k_p = \frac{1}{R} = 4D_{aq}n_p r_p\left[\left(1+\frac{4h_{sc}}{\pi r_p}\right)\frac{D_{aq}}{D_v}+\frac{D_{aq}}{K_s D_s}\right]^{-1} \qquad \text{Eq 9}$$

where D_{aq} is the drug's aqueous diffusion coefficient. It is interesting to note that k_p and therefore the flux through compromised skin is proportional to r_p (providing that $r_p \geq h_{sc}$) and not r_p^2, as would have been expected for the intuitive model in which transport is proportional to the total area of pores. In the latter case, the permeability through porated SC would equal that across skin with no functional barrier multiplied by the fractional pore area (A_{pore}/A_{total}):

$$k_{p\,\mathrm{int}} = \frac{1}{R_{noSC}}\frac{A_{pore}}{A_{total}} = D_{aq}n_p\pi r_p^2\left(h_v\frac{D_{aq}}{D_v}+h_s\frac{D_{aq}}{K_s D_s}\right)^{-1} \qquad \text{Eq 10}$$

Eq 10 is derived from Eq 2 for R_{noSC} and $A_{pore}/A_{total} = n_p\pi r_p^2$. Note that Eq 10 (but with h_v replaced with $h_v + h_{sc}$) can also be obtained by using $a(x) = n_p\pi r_p^2$ in the integral Eq 3 for all values of x.

The flux proportionality to r_p rather than r_p^2 for thin porated membranes is well-known and explains why water evaporation from a leaf is so high (about half of that expected from a fully exposed surface), even though the open surface area of the stomata of plant leaves is only about 1% of the total leaf area [11].

Eq 9 can be further simplified by assuming that $D_v \sim D_{aq}$, which can be deduced from the Wilke–Chang relationship [12]:

$$D_v \approx D_{aq} \approx 7.4\times10^{-8}\frac{\sqrt{2.6MW_w}T}{\eta_w V^{0.6}}\left(cm^2 s^{-1}\right) \qquad \text{Eq 11}$$

where MW_w is the molecular weight of water (18 Da), T is the absolute temperature (305K or 32°C on the skin surface), η_w is the water viscosity (0.77 cP at 305K) and V is the molar volume of the drug at its boiling point (in $cm^3 mole^{-1}$). In the calculations below, V is replaced by the drug's MW (i.e., a density of 1 g cm^{-3} is assumed) and Eq 11 reduces to:

$$D_v \approx D_{aq} \approx 2.0\times10^{-4} MW^{-0.6}\left(cm^2 s^{-1}\right) \qquad \text{Eq 12}$$

The viable skin has been likened to an aqueous gel and it has been suggested that drug diffusivity here is about one-sixth of that in water [13]; it has therefore been assumed that $D_{aq}/\left(K_s D_s\right) \approx 6$. Eq 9 can now be simplified accordingly: if (as is the case experimentally) a typical pore diameter is between 10 and 200 μm, and assuming an SC thickness of 15 μm, then the term in parenthesis in Eq 9 has a value somewhere between 7 and 10. Using 8 as a reasonable compromise given the number of estimates already made, and calculating D_{aq} with Eq 12 (having converted to units of cm^2 h^{-1}), the model predicts the following expressions for the permeability coefficient (in cm h^{-1}) and the flux of the drug through porated skin:

$$k_p \approx 0.36 n_p r_p MW^{-0.6} \qquad \text{Eq 13}$$

$$J = k_p C_v \approx 0.36 n_p r_p MW^{-0.6} C_v \qquad \text{Eq 14}$$

Using the same approximations, the corresponding expressions for the intuitive model are:

$$k_{p\,\mathrm{int}} \approx \frac{2.3}{6h_s + h_v} n_p r_p^2 MW^{-0.6}; \quad J_{\mathrm{int}} = \frac{2.3}{6h_s + h_v} n_p r_p^2 MW^{-0.6} C_v \qquad \text{Eq 15}$$

Ultimately, these permeability coefficients can be compared with the approximation of that through skin which has no SC whatsoever, i.e.:

$$k_{noSC} = \frac{1}{R_{noSC}} = D_{aq}\left(h_v + h_s\frac{D_{aq}}{K_s D_s}\right)^{-1} \approx \frac{0.72}{6h_s + h_v} MW^{-0.6} \qquad \text{Eq 16}$$

In Eqs 13-16, the units for r_p, h_s and h_v are cm and, for n_p, cm^{-2}.

Results and discussion

By way of illustration, Figure 2 compares the predicted skin permeability coefficients for an example small drug (*MW* = 300 and log *P* = 2) using the new and intuitive (area-based) models (Eqs 13 and 15, respectively) as a function of both the number of pores (n_p) and of the fractional pore area (A_{pore}/A_{total}); the calculations have assumed values of $r_p = 25\ \mu$m and $h_s = h_v = 300$ µm. The limiting permeability coefficient values of fully intact SC, determined using the Potts & Guy equation [14], and of skin with no SC whatsoever (k_{noSC}, Eq 16) are also included in the Figure. The value of h_s was chosen on the basis of the situation *in vivo*, and the known ultrastructure and organisation of the dermal microcirculation [15]. The thickness of the dermis is on the order of 1 mm and, while the capillary loops in the dermal papillae (right beneath the epidermal-dermal junction) may not be expected to fully clear all drug arriving from the epidermis, the rich plexus of blood vessels situated a few hundred microns further down [15] is a reasonable location where 'sink' conditions may be expected. *In vitro*, the value of h_s depends on the type of skin used (dermatomed versus full-thickness) and is typically 500-1000 µm as there is no functional microcirculation in this case. In the final approximation of the model (Eqs 12 and 13), the principal contribution to the diffusional resistance is from inside the funnels, and any increase in resistance due to a larger h_s is assumed negligible.

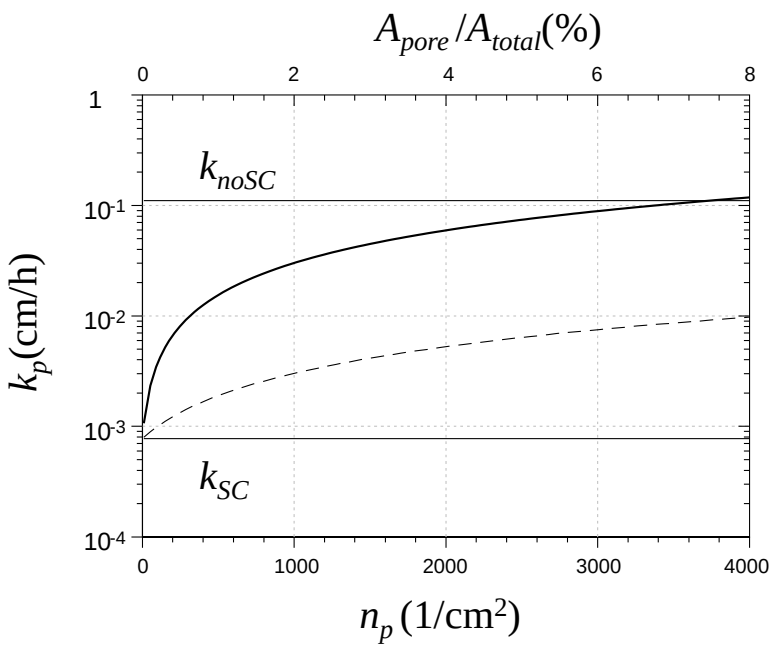

Fig 2. Predicted permeability coefficients of a model small drug as a function of the number of pores (n_p) based on both the new model described in this work (solid line), and an estimate based on an intuitive, area-based calculation (dashed line). Horizontal lines show the limiting cases of the permeability coefficients for fully intact (k_{SC}) and fully compromised SC (k_{noSC}).

It is immediately apparent from Figure 2 that the new approach predicts a permeability coefficient that is approximately an order of magnitude greater than the intuitive estimate. Also, for the same model drug, the new model predicts that the porated skin presents no functional barrier (i.e., $k_p \geq k_{noSC}$) once about 8% of the SC is ablated (equivalent to about 4000 pores per cm^2, in this case). Of course, the situation where $k_p > k_{no\ SC}$ is physically impossible, as the permeability of porated skin can only approach that of the skin with all the SC removed. This violation is due to the pore density exceeding that required by Eq 7 (the right hand side is about 2000 pores per cm^2), and indicates the limit of applicability of the new model.

To assess the validity of the new model, it was used to predict published experimental results [16-21] for a variety of drugs permeating across mammalian skin that had been fully porated either using microneedles or by laser ablation; the measured values were also compared to estimates from the intuitive model and the results are presented in Tables 1 and 2. For laser-porated skin, the pore diameter was reported; in the case of microneedle poration, the pore radius (r_p) was calculated from geometric considerations:

$$r_p = \frac{d_n}{2}\frac{l_{in}}{l_n} \qquad \text{Eq 18}$$

where d_n is the diameter of the microneedle base, l_{in} is the length of that part of the microneedle inserted into the skin, and l_n is the total microneedle length (Figure 3). It has been reported that the depth of the conduits created by microneedles is 40-80 μm [17] and it was therefore assumed, in the predictions summarized in Tables 1 and 2, that l_{in} could be reasonably approximated to a value of 50 μm.

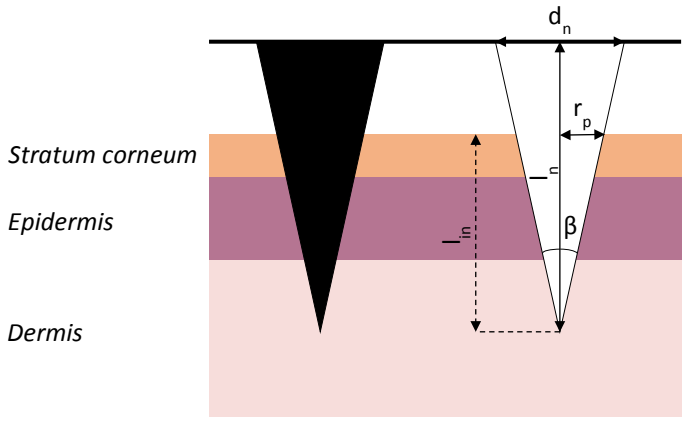

Fig 3. Geometric parameters associated with insertion of a single microneedle into the skin.

The experimental results in Tables 1 and 2 are, in general, better predicted by the new model than the intuitive, area-based approach. This is illustrated graphically in Figure 4 which (for both microneedle and laser poration) shows the ratio of predicted to experimental fluxes for a wide range of drugs. In the case of the new model (red bars), the ratio mostly falls within a factor of 5 of unity (i.e., $0.2 < \text{ratio} < 5$) whereas, for the intuitive estimation (blue bars), the ratio is nearly always less than 0.2. It follows that the novel model described in this research provides a closer description of the measured fluxes of drugs of diverse physicochemical properties across porated skin. The approach may be valuable, therefore, in drug selection and in the design and optimisation of formulation strategies for transdermal delivery through selectively compromised skin.

Figure 4 shows that the new model accurately predicts the experimentally observed fluxes for many compounds across microneedle-porated skin based on logical and readily available parameters, such as the permeant's molecular weight, its concentration in the applied formulation, and the density and radius of the pores. Earlier publications have indicated that a chemical's flux through microneedle-porated skin depends on the length [16], tip radius (sharpness) [22], base width [16], duration of application [23] and insertion force of microneedles [24]. Given the model derived here, these parameters are those which most directly influence the average radius of the created pores.

Flux predictions based on Equation 14 are particularly good for the peptides and proteins (carnitine, hexapeptide, Ac-hexapeptide, oxytocin, cytochrome C, and BSA) that have been investigated experimentally. Equally, good agreement is seen for two conventional, small molecular weight drugs, namely acyclovir and lidocaine. In contrast, the predictions for insulin, diclofenac, rhGH and FSH deviated by a factor of 5 or more from the measured values; in fact, for the latter three compounds, the intuitive model was a better predictor. While the lack of agreement for insulin may be, at least in part, due to the animal model used (rat abdominal skin), the exact reason(s) behind these examples of poor prediction remain, for now, unclear.

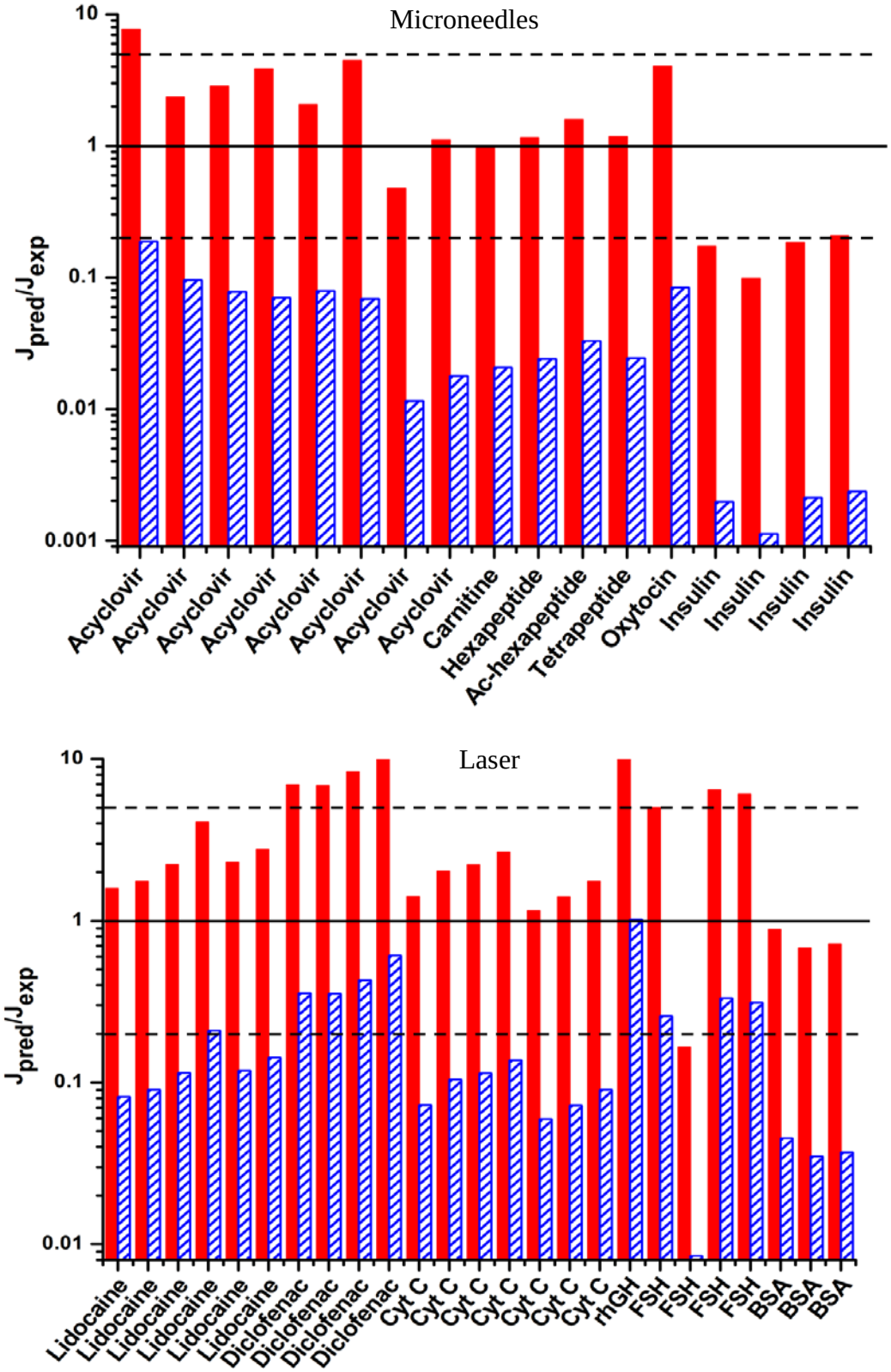

Fig. 4. Ratio of predicted to experimental fluxes using the new model described here (red bars) and the intuitive, area-based approach (blue bars). Data are provided in Tables 1 and 2.

Conclusion

A new, relatively straightforward model has been developed to predict drug permeability through microporated mammalian skin. The approach suggests that drug flux is greater through the compromised barrier than that indicated by a simple, intuitive, area-based model. The validity of the new description was demonstrated by the generally excellent agreement between the model's predictions and published experimental data; in contrast, the intuitive estimates almost always under-estimated (by at least a factor of 5) the measured results. Overall, the new model provides additional insight into the initial conception and development of transdermal delivery approaches across a deliberately and quantitatively deranged skin barrier.

References

[1] K.A. Walters, M.S. Roberts, The structure and function of skin, Drugs and the pharmaceutical Sciences, 119 (2002) 1-40.
[2] S. Wiedersberg, R.H. Guy, Transdermal drug delivery: 30+ years of war and still fighting!, Journal of Controlled Release, 190 (2014) 150-156.
[3] C.A. Lipinski, F. Lombardo, B.W. Dominy, P.J. Feeney, Experimental and computational approaches to estimate solubility and permeability in drug discovery and development settings, Advanced drug delivery reviews, 64 (2012) 4-17.
[4] H. Marwah, T. Garg, A.K. Goyal, G. Rath, Permeation enhancer strategies in transdermal drug delivery, Drug delivery, 23 (2016) 564-578.
[5] A.K. Banga, Microporation applications for enhancing drug delivery, Expert Opinion on Drug Delivery, 6 (2009) 343-354.
[6] T.R.R. Singh, C. Gujral, R.F. Donnelly, Microporation for Enhanced Transdermal Drug Delivery, Novel Delivery Systems for Transdermal and Intradermal Drug Delivery, (2015) 163-178.
[7] Y.A. Gomaa, D.I. Morrow, M.J. Garland, R.F. Donnelly, L.K. El-Khordagui, V.M. Meidan, Effects of microneedle length, density, insertion time and multiple applications on human skin barrier function: assessments by transepidermal water loss, Toxicology in Vitro, 24 (2010) 1971-1978.
[8] Y. Bachhav, S. Summer, A. Heinrich, T. Bragagna, C. Böhler, Y. Kalia, PLEASE® A promising tool for intraepidermal drug delivery, in: Annual Meeting of the Controlled Release Society, 2008.
[9] H. Kalluri, A.K. Banga, Formation and closure of microchannels in skin following microporation, Pharmaceutical research, 28 (2011) 82-94.
[10] R.J. Scheuplein, I.H. Blank, Permeability of the skin, Physiol Rev, 51 (1971) 702-747.
[11] C.S. Patlak, A contribution to the study of diffusion of neutral particles through pores, The bulletin of mathematical biophysics, 21 (1959) 129-140.
[12] C.R. Wilke, P. Chang, Correlation of Diffusion Coefficients in Dilute Solutions, Aiche Journal, 1 (1955) 264-270.
[13] R.J. Scheuplein, I.H. Blank, Mechanism of percutaneous absorption IV. Penetration of non electrolytes (alcohols) from aqueous solutions and from pure liquids, J Invest Dermatol, 60 (1973) 286--296.
[14] R.O. Potts, R.H. Guy, Predicting skin permeability, Pharmaceutical research, 9 (1992) 663-669.

[15] I.M. Braverman, The cutaneous microcirculation: ultrastructure and microanatomical organization, Microcirculation, 4 (1997) 329-340.
[16] G. Yan, K.S. Warner, J. Zhang, S. Sharma, B.K. Gale, Evaluation needle length and density of microneedle arrays in the pretreatment of skin for transdermal drug delivery, International journal of Pharmaceutics, 391 (2010) 7-12.
[17] S. Zhang, Y. Qiu, Y. Gao, Enhanced delivery of hydrophilic peptides in vitro by transdermal microneedle pretreatment, Acta Pharmaceutica Sinica B, 4 (2014) 100-104.
[18] Y. Wu, Y. Gao, G. Qin, S. Zhang, Y. Qiu, F. Li, B. Xu, Sustained release of insulin through skin by intradermal microdelivery system, Biomedical microdevices, 12 (2010) 665-671.
[19] Y. Bachhav, S. Summer, A. Heinrich, T. Bragagna, C. Böhler, Y. Kalia, Effect of controlled laser microporation on drug transport kinetics into and across the skin, Journal of Controlled Release, 146 (2010) 31-36.
[20] Y.G. Bachhav, A. Heinrich, Y.N. Kalia, Using laser microporation to improve transdermal delivery of diclofenac: increasing bioavailability and the range of therapeutic applications, European Journal of Pharmaceutics and Biopharmaceutics, 78 (2011) 408-414.
[21] Y. Bachhav, A. Heinrich, Y. Kalia, Controlled intra-and transdermal protein delivery using a minimally invasive Erbium: YAG fractional laser ablation technology, European Journal of Pharmaceutics and Biopharmaceutics, 84 (2013) 355-364.
[22] C.S. Kolli, A.K. Banga, Characterization of solid maltose microneedles and their use for transdermal delivery, Pharmaceutical research, 25 (2008) 104-113.
[23] Y. Wu, Y. Qiu, S. Zhang, G. Qin, Y. Gao, Microneedle-based drug delivery: studies on delivery parameters and biocompatibility, Biomedical microdevices, 10 (2008) 601-610.
[24] K. Cheung, T. Han, D.B. Das, Effect of force of microneedle insertion on the permeability of insulin in skin, Journal of diabetes science and technology, 8 (2014) 444-452.

Table 1: Experimental and predicted fluxes of various drugs through microneedle-porated skin

Drug (*MW*, Da)	**Skin**	**h_s (μm)**	**C_v (μg mL^{-1})**	**n_p (cm^{-2})**	**d_n (μm)**	**l_n (μm)**	**r_p (μm)[a]**	**J_{expt} (μg cm^{-2} h^{-1})**	**$J_{intuitive}$ (μg cm^{-2} h^{-1})**	**J_{model} (μg cm^{-2} h^{-1})**	**Ref.**
Acyclovir (225)	Human epidermal membrane	200	1600	2000	92	400	5.8	3.4	0.63	25.7	[16]
				400	250	650	9.6	3.7	0.35	8.59	
				900	167	650	6.4	4.5	0.35	12.9	
				2000	112	650	4.3	5.0	0.35	19.2	
				400	306	850	9.0	3.9	0.30	8.04	
				2000	124	850	3.7	3.7	0.25	16.3	
				400	250	1100	5.7	10.7	0.12	5.08	
				900	167	1100	3.8	6.9	0.12	7.63	
L-Carnitine (161)	Porcine ear, split-thickness	800	14508	756	100	150	16.7	314 ± 34	6.5	312	[17]
Hexa-peptide (499)			44874					410 ± 41	9.9	490	
Acetyl-hexa-peptide-3 (889)			80010					391 ± 124	12.9	617	
Tetrapeptide-3 (457)			41094					419± 54	10.2	473	
Oxytocin (1007)			90648					161 ± 50	13.6	649	
Insulin[b] (5960)	Rat abdomen, full-thickness	1500	200	484	100	150	16.7	1.8 ± 0.4	0.004	0.32	[18]
			350					5.6 ± 0.4	0.006	0.55	
			740					6.3 ± 1.0	0.013	1.17	
			920					7.0 ± 3.1	0.017	1.45	

[a] Pore radius calculated using Eq 18. [b] FITC-labelled insulin; experimental flux determined from amount penetrated in 3 hours.

Table 2: Experimental and predicted fluxes of various drugs through laser-porated skin.

Drug (*MW*, Da)	**Skin**	**h_s (μm)**	**C_v (μg mL^{-1})**	**n_p (cm^{-2})**	**r_p (μm)**	**J_{expt} (μg cm^{-2} h^{-1})**	**$J_{intuitive}$ (μg cm^{-2} h^{-1})**	**J_{model} (μg cm^{-2} h^{-1})**	**Ref.**
Lidocaine (234)	Porcine ear, full-thickness	1500	10000	50	75	32 ± 4.6	2.63	51.1	[19]
				100		58 ± 18	5.27	102	
				150		69 ± 18	7.90	153	
				300		75 ± 27	15.6	306	
			25000	150		167 ± 58	19.8	383	
	Human, full-thickness		10000	300		111 ± 8.7	15.7	306	
Diclofenac (296)	Porcine ear, full-thickness		10000	50		6.4 ± 4.4	2.29	44.4	[20]
				100		13 ± 4.4	4.58	88.8	
				150		16 ± 6.1	6.86	133	
				300		22 ± 3.3	13.7	266	
Cytochrome C[a] (12400)			1000	300		2.0 ± 0.37	0.15	2.83	[21]
				100		0.47 ± 0.10	0.049	0.95	
				150		0.64 ± 0.49	0.073	1.42	
				600		2.1 ± 0.66	0.29	5.67	
			5000	300		12 ± 1.4	0.73	14.2	
rhGH[b] (22000)			3300	300		0.34 ± 0.18	0.34	6.69	
FSH[c] (30000)			25	300		0.008 ± 0.004	0.002	0.04	
			165			1.7 ± 0.02	0.014	0.28	
			330			0.09 ± 0.03	0.028	0.55	
			666			0.19 ± 0.02	0.057	1.11	
BSA[d] (70000)			10000	300		11.4 ± 1.3	0.52	10.0	
						14.8 ± 3.7	0.52	10.0	
						14.0 ± 4.6	0.52	10.0	
Cytochrome C[a] (12400)	Human, full-thickness		1000	300		2.0 ± 0.78	0.15	2.83	
						1.6 ± 0.34	0.15	2.83	

[a] Equine heart cytochrome C. [b] Recombinant human growth hormone. [c] Urinary follicle stimulating hormone. [d] FITC-labelled bovine serum albumin.